Universitat Politècnica de Catalunya (UPC)
Universitat Autònoma de Barcelona (UAB)
Universitat de Barcelona (UB)
Institut de Ciències Fotòniques (ICFO)

http://www.photonicsbcn.eu

Master in Photonics

MASTER THESIS WORK

Resonances in Graphene Plasmons

David Alcaraz Iranzo

Supervised by Prof. Frank Koppens, (ICFO)
&
Dr. Sebastien Nanot, (ICFO)

Presented on date 9th September 2014

Registered at

Escola Tècnica Superior d'Enginyeria de Telecomunicació de Barcelona

Resonances in Graphene Plasmons

David Alcaraz Iranzo

ICFO - The Institute of Photonic Sciences, Parc Mediterrani de la Tecnologia, Av. Carl Friedrich Gauss, 3, 08860 Castelldefels (Barcelona), Spain

E-mail: david.alcaraz@icfo.es

August 2014

Abstract. Graphene is used as a novel, versatile plasmonic material. The most common way to implement resonant light-plasmon coupling is to etch graphene into periodic nanostructures, which is invasive. Here, we study a non-invasive way to engineer graphene plasmon resonance, based on periodic doping profiles. The plasmon resonances are calculated by performing numerical simulations. In addition, we report on simulations of near-field resonant coupling between a dipole and graphene plasmons. Finally, preliminary results on the experimental realization of graphene plasmon resonances are reported. This study demonstrates the potential to exploit graphene plasmons for extreme energy confinement which could lead to strong nonlinear effects.

Keywords: graphene, plasmons, nanostructures.

1. Introduction

Graphene is an interesting material for optics and opto-electronics because of its high mobility and tunable broadband absorption. It possesses properties unseen in 3D materials with many potential applications in visible and the mid-infrared (MIR) range like photovoltaics, plasmonics or electro-optical transistors. In this context, graphene plasmonics have attracted specific interest since they allow of in-situ tunable resonant absorption in the terahertz and MIR range. Transmission has been studied theoretically [1, 2] and experimentally, for various types of nanostructures [3, 4]. Moreover, graphene plasmons (GP) exhibit very strong confinement, enabling sub-wavelength manipulation of optical fields. This strong optical field confinement can lead to very strong plasmonic non-linearities, potentially enabling optical switching at the level of a single plasmon [5].

The aim of this work is to design novel techniques to couple light to GP and study their properties, with the ultimate goal to observe the first signatures of the plasmon non-linear response. In this report, the main relevant properties of graphene are described. We introduce two types of experimental probes for GP: 1) the scanning near-field optical microscope (s-SNOM), and 2) far-field optical absorption spectra of nanostructures. In the context of these two experimental probes, we present in this report simulations supporting or predicting existing or future experiments. We show a novel method of resonant plasmon confinement, by introducing periodic doping gradients. Finally, the device design for preliminary and future experiments is explained.

2. Graphene properties

Graphene consists of a two dimensional hexagonal array of carbon atoms with sp^2 hybrid bonds. It is the basic building block of 3D graphite. However, it shows completely different electrical, optical and mechanical properties than its corresponding bulk material, due to the lowering of the dimensionality to the thickness of an atom.

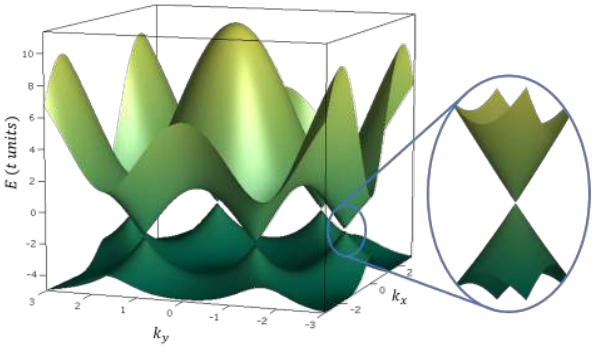

Figure 1: Electronic band structure of graphene's first Brilluoin zone and close up onto one of the Dirac's cones. Horizontal coordinates represent in-plane electron's momentum (in a^{-1} units where $a \sim 230$ pm is the lattice parameter) and vertical the energy in $t \sim 2.9$ eV (tight binding coefficient) units. It is calculated using tight binding model with hoping neighbors equation from [8].

Graphene can be obtained by several methods including exfoliation from graphite (first realization reported in [6]), by chemical vapor deposition (CVD) [7] or epitaxial growth from SiC substrates. Depending on the method, it will present rather different properties. In general, exfoliation provides better quality but smaller graphene flakes than CVD, which is extensively used for large area applications.

2.1. Electronic properties

The electronic properties are governed by graphene's electronic band structure and its doping level. Graphene's electrical peculiarities come from the presence of Dirac's cones in *K* points of the Brillouin zone. In other words, the dispersion relation of the charge carriers around the charge neutrality point is linear as shown in figure 1 inset.

The top cone corresponds to the conduction band (CB) and the bottom one to the valence band (VB). Both touch exactly at the charge neutrality point (CNP), also called Dirac Point. For that reason graphene is a gapless semiconductor or semi-metal. If the Fermi level is in the top cone (CB), charge carriers will consist of electrons; otherwise they will be holes (VB).

Electrons in graphene behave as massless Dirac fermions, which means that their propagation velocity and effective mass are constant and zero, respectively. The linear dispersion relation at the Dirac cone is given by $E = \hbar v_F k$, where $\hbar$ is the reduced Planck's constant, E and k are the electron's energy and momentum and $v_F \approx c/300$ is the Fermi velocity, only a fraction of c, the speed of light, in any in plane direction (figure 1 inset).

The Fermi energy level (E_F) usually resides around the Dirac cones and the Fermi energy dependence on the charge carrier density n_c is:

$$|E_F| = \hbar v_F \sqrt{\pi n_c}. \tag{1}$$

When E_F is positioned exactly at the intersection of both cones, graphene is set at the Dirac point ($E_F = 0$) and the charge carrier density is 0. In electrical transport experiments, a maximum in resistivity is reached at the CNP. This behavior is explained using:

$$\rho = (n_c \mu_c \mathrm{e})^{-1}, \tag{2}$$

where ρ is the electrical resistivity, μ_e is their mobility and e being the fundamental electric charge and equation (1). Hence with no free carriers at the CNP, resistivity ideally diverges to infinity.

2.2. Optical properties

Graphene is a semi-metal and its optical properties can be explained using the optical conductivity model. This means that its permittivity ε can be expressed in the same form as for a metal:

$$\varepsilon = \varepsilon_0 + i\frac{\sigma}{\omega}, \tag{3}$$

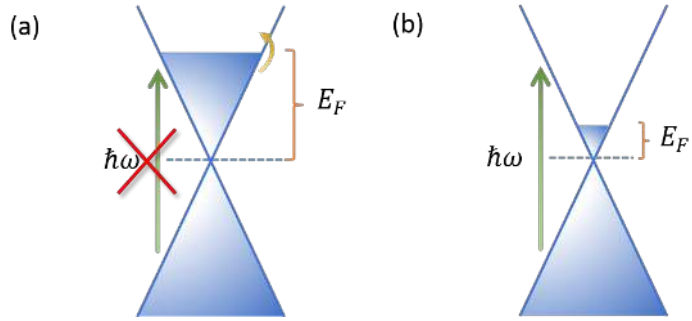

Figure 2: Photon absorption mechanisms in graphene. **(a)** With photon energies $\hbar\omega < 2E_F$ they cannot excite electrons from the valence to the conduction band due to Pauli blocking. Only intra-band absorption occurs (curved line). **(b)** Inter-band absorption is allowed for $\hbar\omega > 2E_F$.

where ε_0 is the vacuum permittivity, ω the optical frequency and σ the optical conductivity.

In terms of optical absorption ($A = \pi\sigma_{tot}/c$) two types of mechanisms can occur: Drude's metallic intra-band absorption and inter-band optical transitions (similar to light absorption in semiconductors). When the photon energy is below $2E_F$ as shown in figure 2(a), graphene behaves as a metal and electrons in the Fermi sea are excited; but above it electron-hole pairs are created, see figure 2(b). These features have been typically observed experimentally and are represented in figure 3(b).

The transition between these two regimes occurs at photon energies around $2E_F$ and as a consequence can be tuned by varying the doping. For lower energies direct transitions are forbidden due to Pauli blocking, they are going to be only possible with phonon contribution. Inter-band absorption in monolayer graphene is constant and its value is $A = \pi\alpha \approx 2.3\%$, where $\alpha = 1/137$ is the fine-structure constant.

Various analytical expressions taking into account the doping and temperature dependence of the optical conductivity are obtained using the random phase approximation (RPA). The optical conductivity plotted in figure 3(a) corresponds to the local RPA in the $k_\parallel \to 0$ limit, which includes the electric dipole approximation (EDA) from [9]. For $T \to 0$ the expression is:

$$\sigma(\omega) = \frac{\mathrm{e}^2 E_F}{\pi\hbar^2}\frac{\mathrm{i}}{\omega + \mathrm{i}\tau^{-1}} + \frac{\mathrm{e}^2}{4\hbar}\left[\theta(\hbar\omega - 2E_F) + \frac{\mathrm{i}}{\pi}\log\left|\frac{\hbar\omega - 2E_F}{\hbar\omega + 2E_F}\right|\right]. \tag{4}$$

The first term represents the intra-band transitions or metallic Drude behavior and the second one the inter-band transitions. The transition between intra and inter-band regimes is broadened by temperature as seen in figure 3(b).

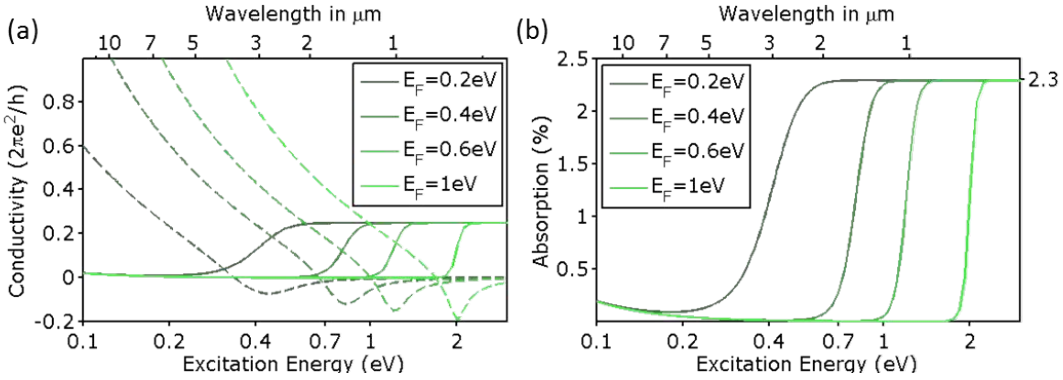

Figure 3: Optical properties of graphene at $300K$ and fixed mobility of $1000\ cm^2/Vs$ for different dopings using [9] local RPA. **(a)** Real (solid line) and imaginary (dashed line) parts of the optical conductivity . **(b)** Light absorption of a single layer of graphene obtained from its optical conductivity; Drude (intra-band) to inter-band behavior transition occurs around $2E_F$.

2.3. Graphene optical nonlinearities

It has been demonstrated experimentally in [10] that graphene possesses non-zero $\chi^{(3)}$ electrical susceptibility by four-wave mixing measurements. Because of their linear band dispersion, electrons traveling at Fermi speed immediately flip direction but not absolute value when the electric field sign is changed. As a consequence, the response to an electromagnetic field varying sinusoidally in time is a square signal. Odd harmonics of the driving field are generated as detailed in [11]. Other authors claim that $\chi^{(2)}$ should also be intrinsically non-zero due to non-local coupling breaking inversion symmetry and could be enhanced by plasmon confinement [5].

3. Plasmon confinement

Surface Plasmon Polaritons (SPP's) or plasmons, are pseudo-particles that arise from the coupling between an electromagnetic wave and the excitations of electrons in the metal, in the form of an electron density wave, at the conductor/insulator interface. Alternatively, plasmons could be seen also as a self-existing solution to Maxwell's equations in the mentioned environment. This solution is found by imposing field continuity at the interface for Transverse Magnetic (TM) fields. The condition to sustain an interface in-plane propagating wave with perpendicular evanescent fields (plasmon) is a negative permittivity in one of the 2 media, i.e. metallic behavior [12].

For a regular metal, it is known that the permittivity takes the form of (3) where:

$$\sigma = \sigma_m = \frac{\omega_p^2 \varepsilon_0}{\tau^{-1} - \mathrm{i}\omega} \qquad \text{and} \qquad \omega_p^2 = \frac{n_e \mathrm{e}^2}{\varepsilon_0 m_\mathrm{e}}, \tag{5}$$

with ω_p being the metal plasma frequency, τ the plasmon lifetime, n_e the electrons density and m_e their mass. From [3] the plasmon wave-vector dependence with material's dielectric functions in an infinite plane interface and introducing (5) read (black line in figure 4):

$$k_p = \frac{\omega}{c}\left(\frac{\varepsilon_m \varepsilon_d}{\varepsilon_m + \varepsilon_d}\right)^{1/2} \qquad \Rightarrow \qquad k_p = \frac{\omega}{c}\left(\frac{\omega^2 - \omega_p^2}{2\omega^2 - \omega_p^2}\right)^{1/2}, \tag{6}$$

where sub-indexes d and m stand for dielectric and metal. If the thickness of the metallic layer is reduced, plasmon solution takes the form of the following equation (blue line in figure 4):

$$\coth\left(\sqrt{k_p^2 - \omega^2 \mu_0 \varepsilon_m}\,\Delta/2\right) = -\frac{\varepsilon_m}{\varepsilon_0}\frac{\sqrt{k_p^2 - \omega^2\mu_0\varepsilon_0}}{\sqrt{k_p^2 - \omega^2\mu_0\varepsilon_m}}, \tag{7}$$

with Δ the metal thickness. If it is decreased, up to a thickness equivalent to a monoatomic layer, the plasmon dispersion relation of a 2D electron gas becomes (orange line in figure 4):

$$\omega_p = D_{2D}\sqrt{k} \qquad \text{where} \qquad D_{2D} = \left(\frac{2\pi \mathrm{e}^2 n_{2D}}{\epsilon_0 m^*}\right)^{1/2}, \tag{8}$$

being n_{2D} the 2-dimensional electron density and m^* their effective mass. If the material is then changed to graphene, its plasmons dispersion relation for massless electrons is then given by (red line in figure 4):

$$\omega_p = D_G\sqrt{k} \qquad \text{, where} \qquad D_G = \sqrt{\frac{\pi \mathrm{e}^2 v_F n^{1/2}}{\epsilon_0 \hbar}}. \tag{9}$$

This expression is easily simplified using (1) in the regime of low excitation energies in comparison to the Fermi energy ($E_F > \hbar\omega$) as deduced in [14] to:

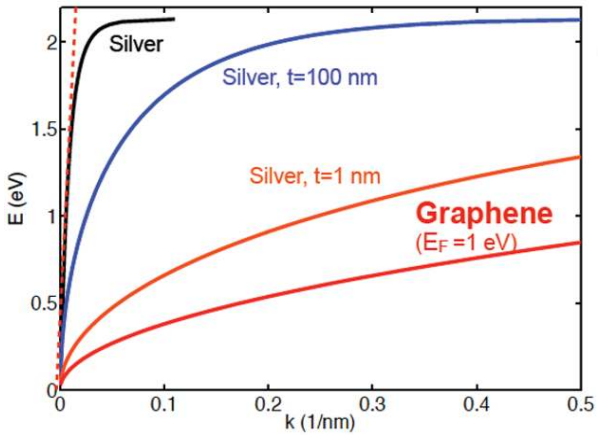

Figure 4: Pasmon dispersion relation for different silver thicknesses and graphene, both in vacuum. Red dashed line is the vacuum light line. Figure taken from F. Koppens' presentation.

$$\frac{\lambda_{sp}}{\lambda_0} \approx \frac{4\alpha}{\varepsilon_1 + \varepsilon_2} \frac{E_F}{\hbar\omega}, \tag{10}$$

where λ_0 stands for the vacuum wavelength, λ_{sp} for the GP one and ε_1 and ε_2 being the dielectric constants of the materials above and below graphene. It can be deduced from (10) that light energy confinement in GP form is extremely high, achieving up to 2 orders of magnitude wavelength reduction, whereas in regular metals $\lambda_0/\lambda_{sp} \sim 3$.

4. Resonances of Graphene Plasmons

One talks about resonances when at a given frequency and position of a source, any observable in the sample is enhanced due to phase addition effects. Thus it is possible to talk about two different kinds of resonances in the case of plasmon-polaritons (i.e. when plasmons are coupled to an electromagnetic wave): far and near-field ones. In far-field optical resonances, the excitation source is a plane wave, where the important parameters are the propagation direction, their frequency and polarization. However, in the near-field, plasmons are coupled directly to evanescent waves and frequency, position and orientation of the source are parameters of equal importance.

Far-field couples resonantly to plasmons by nanostructuring graphene. For simple geometries like circles, rectangles or ribbons, if they are isolated, resonance is established because of GP reflection at the edge. The phase condition from [13] to be fulfilled is:

$$2\pi \frac{W}{\lambda_{sp}} + 2\Phi_R = 2\pi n. \tag{11}$$

Here, W is the desired direction width, Φ_R is the reflection phase change and $(n+1)$ is the resonant mode order. In the case of ribbon arrays, the electrical TM field (perpendicular to the ribbon's axis) is confined inside graphene, except the low order ones that can be coupled through the whole structure. These resonances are observed in the far-field as absorption peaks in the transmission spectrum.

In the case of near-field resonances, a typical tool is the s-SNOM techniques. This method is a scanning probe technique, providing a map of the local density of optical states, as discussed in [14]. It consist in illuminating with an IR laser a metal coated atomic force microscope (AFM) tip, whose evanescent fields couple to GP. Those GP propagate and eventually are reflected back from the boundaries or obstacles. The plasmonic interference evanescent tail under the AFM tip is coupled back to the detector as back-scattered light. This signal is related with the Purcell factor [15]: the ratio between the power radiated by a punctual emitter (a dipole, fluorescent molecule, etc.) in a certain position close to the sample and the emission of the same emitter in vacuum.

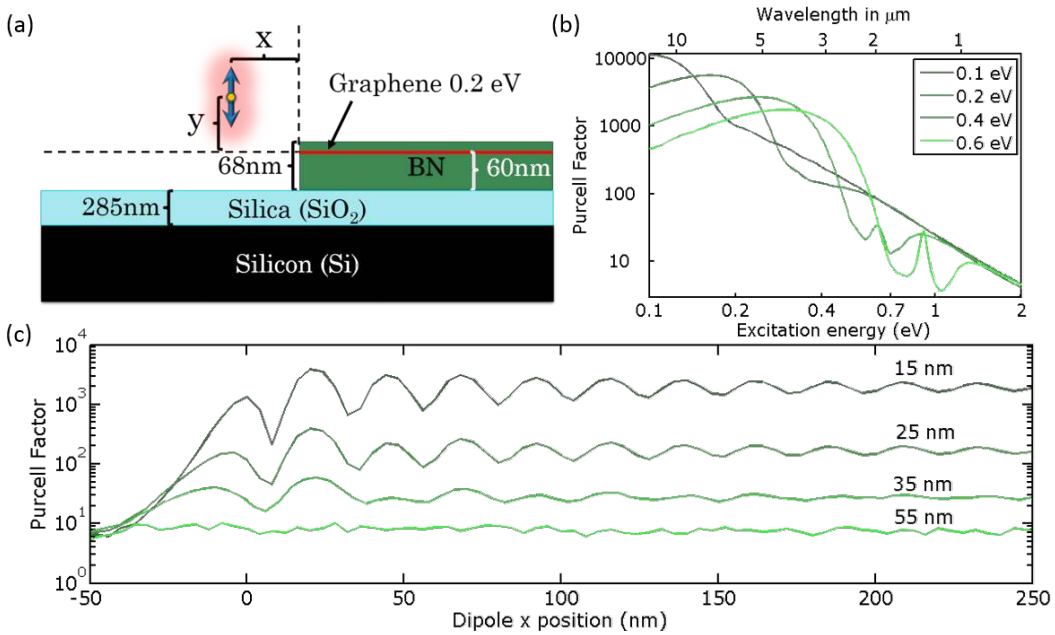

Figure 5: Purcell factor simulation. **(a)** 2D FDTD Lumerical dipole excitation simulation scheme of the s-SNOM experiment. It consists in boron nitride (BN) encapsulated graphene on a silicon and silica substrate. **(b)** Purcell factor of a dipole at 10 nm of suspended graphene at different dopings as in [9]. **(c)** Purcell factor position dependence of a 10.6 μm emission wavelength dipole at several heights and perpendicular to graphene.

5. Simulations

Simulations are performed in 2D using Lumerical, a finite differences in time domain (FDTD) software solution. This solves EM fields propagation based on Maxwell's equations in a discretized space-time. It does provide both time-dependent and steady state results by Fourier transforming. Simulations with graphene quickly become extremely time consuming. First, because graphene's proper dimensions (thickness below 1 nm) force to introduce a mesh size smaller than that. Then, because the plasmon wavelength of graphene is up to 2 orders of magnitude smaller than the free space wavelength, this increases the simulation time even further. And finally, graphene does not have absolute properties; they depend on the fabrication method (mobility), temperature (scattering) and doping (number of carriers), and they have to be introduced into the model to obtain the corresponding optical properties for each minor change.

5.1. Near Field

One of the goals of this project is to reproduce the expeirmental s-SNOM nano-imaging experiment performed on h-BN encapsulated graphene (on a Si/SiO2 substrate). We simulate the plasmon launching by scattering on the AFM tip as a vertical dipole [14] and the signal measured corresponding to each position is (by approximation) proportional to the Purcell factor, as shown in figure 5(a). To validate the simulation parameters, the Purcell factor for a wide range of energy of a dipole perpendicular to an infinite graphene sheet at 10 nm distance simulations are plotted in figure 5(b). They show qualitative agreement with [9] except for an artifact in the transition from intra to inter-band absorptiondue to simplified modeling of temperature dependent optical conductivity, which does not affect the 10.6 μm range.

Figure 5(c) shows the simulations of the Purcell factor for a range of positions and heights. Interestingly, the results show the double fringes pattern, around 35 nm, already seen in the group's experiments (to be published). The shorter wavelength oscillations come

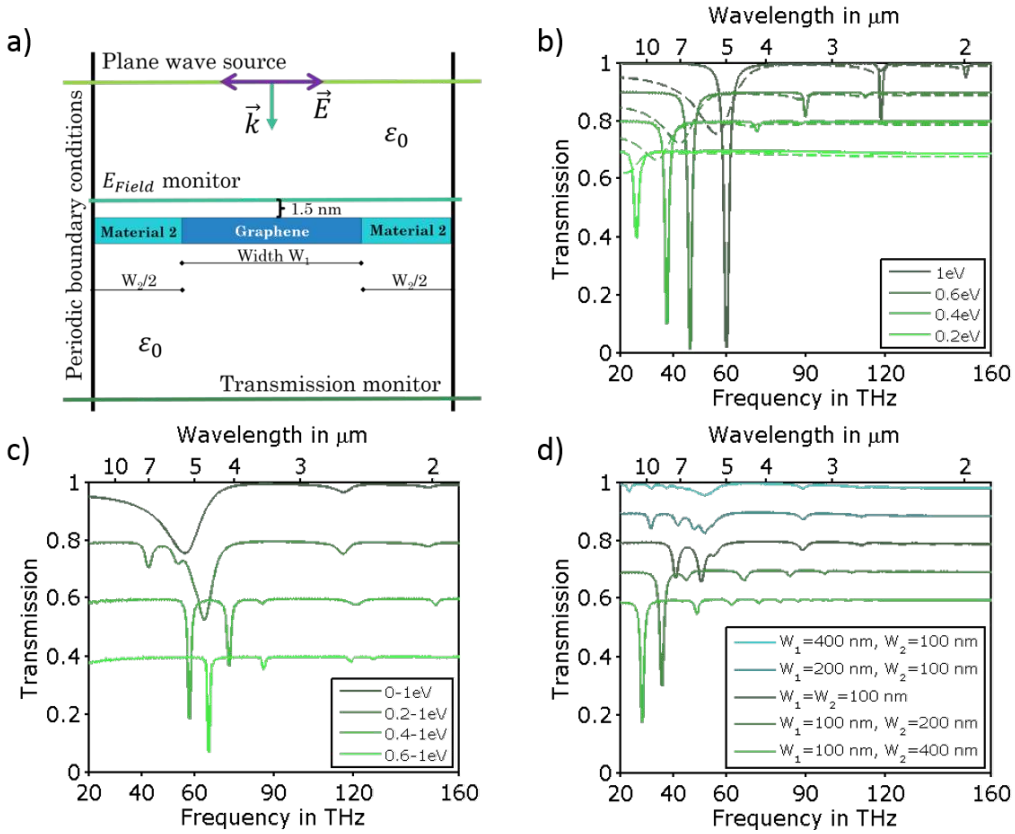

Figure 6: Simulated nanoribbon transmissions. **(a)** 2D FDTD Lumerical transmission simulation scheme. Material 2 is either air or graphene. $W_1 = W_2 = 100$ nm in the simulations unless otherwise stated. **(b)** Ribbons absorption resonances for several dopings of graphene and for material 2 being air (solid lines) or undoped graphene (dashed lines). **(c)** Resonances of 1 eV ribbons varying the doping of region 2 graphene. **(d)** Width dependence resonances evolution of 0.2 (material 1) and 0.6 eV graphene (material 2) doping gradient ribbons. Lines are offset for clarity in (b), (c) and (d).

from direct coupling of the dipole to GP under the tip (direct launching) and interference of the plasmons reflecting from the edge through the tip back into photons. Conversely, the long wavelength oscillations are due to the coupling of the dipole directly to the edge (edge launching) and from the edge, plasmons propagate through graphene and couple to the tip. Thus, in the later, the wavelength is exactly double than the former, travelling only once through graphene, while the directly launched plasmon travels twice the distance. The edge launching component decays for increasing dipole-edge distance. The direct launching is constant, but due to the decay length of GP the signal oscillations are weaker. The double fringes pattern is given when an equilibrium of both launching mechanisms is reached at a certain height.

5.2. Far Field

The objective is to simulate GP resonances in doping gradient ribbons in order to support the design of the experimental implementation. The periodic configuration in figure 6(a) has been used. The source is a set of plane waves covering the spectral region of interest. Transmission is observed far away from the graphene ribbons and the spectral near-field distribution is taken in a line field monitor at 1.5 nm above them. A central region of width W_1 is used to define graphene ribbons. Air or graphene with a different doping (doping step gradient ribbons) are used to separate ribbons (with a width of $W_2/2$ at each side). A periodic structure is obtained

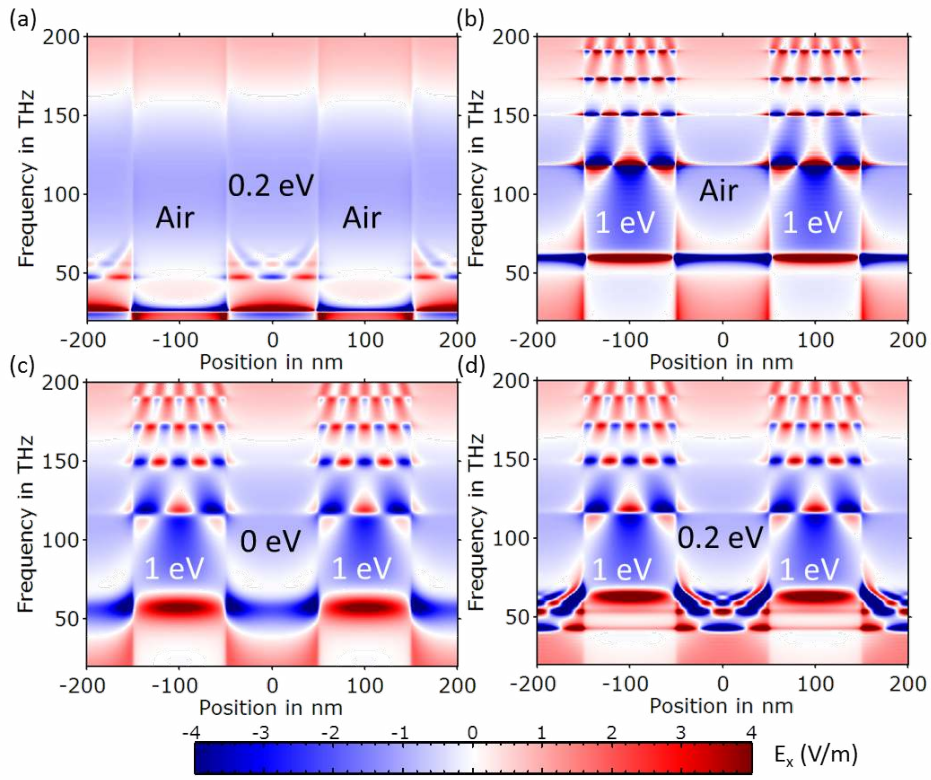

Figure 7: Field modes of the in plane electric field component perpendicular to the ribbons. **(a)** 0.2 eV graphene ribbons in air. **(b)** 1 eV graphene ribbons in air. **(c)** 1 eV and undoped graphene ribbons. **(d)** $0.2 - 1$ eV graphene ribbons. Color scale is shared for all the plots.

introducing periodic boundary conditions over $W_1 + W_2$. In the simulations the substrate was not introduced for simplicity.

The transmission spectra are depicted by solid lines in figure 6(b) for a periodic array of suspended graphene ribbons with different doping. GP resonances are a confined electromagnetic field distribution caused by reflections in nanostructured graphene edges, producing absorption peaks in the transmission spectra. It is clearly seen that the main resonance (the first mode) blue-shifts with increasing doping in agreement with (10). Absorption is also enhanced with increasing doping because there are more charge carriers to enforce the resonance (to couple with).

When introducing undoped graphene to define the ribbons instead of air [dashed lines in 6(b)], the resonant modes in doped graphene are due to reflections at the doping gradient. They couple with the continuum of inter-band transition states. This induces a stronger inter-ribbons coupling giving rise to red shift together with a plasmon damping and interferences which produce an asymmetric lineshape known as a Fano resonance [16].

A spectral distribution of E_x (the electric field component perpendicular to the ribbons axis) of 0.2 and 1 eV graphene ribbons in air through 2 periods are shown in figure 7 (a) and (b). It is seen that the field distribution shows an odd number on anti-nodes because far-field cannot couple to even modes. GP resonant modes finish at a frequency where their decay length is smaller than half the ribbon width. Then, up to the frequency equivalent to $2E_F$, GP are confined at the ribbon edge. In figure 7(c) the same case as in (b), but with undoped graphene instead of air, is shown. The field distribution justifies the above mentioned effects: broadening and damping through plasmon inter-ribbon coupling.

Following the procedure, undoped graphene is replaced by doped graphene and several

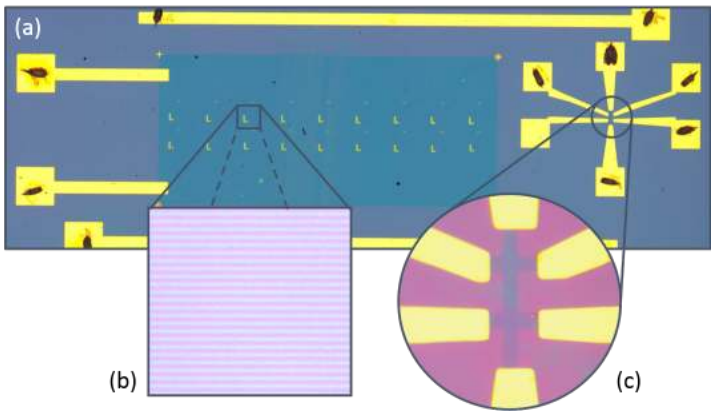

Figure 8: Device optical image with magnified details. **(a)** Complete device with connexions. Close-ups of PMMA nano-ribbons. **(b)** and graphene Hall bar **(c)**.

combinations are run. Transmission spectra in figure 6(c) illustrate how the resonance conditions are changed for various doping level contributions. New coupled modes appear when both ribbons can hold GP, varying the resonance absorption peaks. The 60 THz (1 eV) absorption peak couples to low doping ribbons higher resonant modes. As the doping of the second ribbon approaches to 1 eV, the main mode couples with lower order modes until both fundamental modes start coupling. For high energies, the highly doped ribbon intra-band modes couple to the low-doped ribbon inter-band region similarly as they do with undoped graphene. All those effects can be seen in figure 7(d).

Simulations representing the effect of the width are shown in figure 6(d), confirming ribbon size as a plasmon tuning tool. As expected, the larger the width, the larger the red-shift in the absorption peaks, as seen in (11). The width of the ribbon increasis its relative weight if the other ribbon width is fixed. Here the resonant condition involve both ribbons and create mixed modes.

6. Experimental Realization

In experiments, patterned CVD graphene on a Si-SiO_2 MIR transparent wafer devices (see figure 8) were studied. It comprises a CVD graphene rectangle area where nano-ribbons are patterned in the marked zones (b) for Fourier transform infrared spectroscopy (FTIR) measurements; a graphene Hall bar (c) and gold electric contacts to carry out electrical measurements. The Fermi energy is tuned by using the silicon wafer as the back-gate to charge graphene by capacitive means in the transistor configuration. Nano-ribbons are typically fabricated by lithographic processes and etching, but those imply too many edge imperfections (technique resolution limit) for the length scale needed. Then a non invasive way of patterning ribbons in graphene has been tried: the doping gradient. The approach is based on patterning of nano-ribbons into some other material on top of graphene (PMMA trials until now) and then spincoat (to obtain an optically flat surface) polymer as a topgate in order to create the potential gradient inside graphene.

The electrical measurements serve to determine carrier type, density and mobility (to know E_F) through I(V) curves and Hall measurements (involving magnetic fields) and their back and top-gate dependence. Those measurements are used to control doping during FTIR measurements and tune plasmon resonances.

It should be commented that no remarkable results have been achieved regarding doping gradient ribbons by the moment but preliminary results on etched ribbons reproduce the trend reported in the literature.

7. Conclusion

This work demonstrates that graphene doping gradient can be used as a tool for confining and tuning GP resonances without inducing edge effects or defects in graphene. It has also been

established a plausible mechanism for the BN encapsulated graphene double fringes observed in s-SNOM measurements, explained by edge launching in addition to typical s-SNOM direct launching. For future work, we propose to take advantage of the ultra-high confinement of the EM energy in GP to achieve optical nonlinearities at low excitation power. This will be studied both experimentally and through simulations.

Acknowledgments
I would like to thank my thesis advisor Professor F. Koppens and Dr. S. Nanot for their supervision of this work and Dr. M. Lundeberg and Mr. A. Woessner for their collaboration and useful discussion. I would also like to show my gratitude to the rest of the people in Nano-optoelectronics group at ICFO for their patience and help.

References

[1] Z. Fang, Y. Wang, A. E. Schlather, Z. Liu, P.l M. Ajayan, F. J. García de Abajo, P. Nordlander, X. Zhu, and N. J. Halas, *Active Tunable Absorption Enhancement with Graphene Nanodisk Arrays*. Nano Letters 2014 14 (1), 299-304.

[2] S. Thongrattanasiri, F. H. L. Koppens, and F. J. García de Abajo, *Complete Optical Absorption in Periodically Patterned Graphene*. Phys. Rev. Lett. 108, 047401.

[3] T. Low and P. Avouris, *Graphene Plasmonics for Terahertz to Mid-Infrared Applications*. ACS Nano 2014 8 (2), 1086-1101.

[4] V. W. Brar, M. S. Jang, M. Sherrott, J. J. Lopez, and H. A. Atwater, *Highly Confined Tunable Mid-Infrared Plasmonics in Graphene Nanoresonators*. ACS Nano 2014 8 (2), 1086-1101.

[5] M. Gullans, D. E. Chang, F. H. L. Koppens, F. J. García de Abajo, and M. D. Lukin, *Single-Photon Nonlinear Optics with Graphene Plasmons*. Phys. Rev. Lett. 111, 247401.

[6] K. S. Novoselov, A. K. Geim, S. V. Morozov, D. Jiang, Y. Zhang, S. V. Dubonos, I. V. Grigorieva, and A. A. Firsov, *Electric Field Effect in Atomically Thin Carbon Films*. Science 22 October 2004: 306 (5696), 666-669.

[7] C. Mattevi, H. Kim a and M. Chhowalla, *A review of chemical vapour deposition of graphene on copper*. J. Mater. Chem., 2011, 21, 3324-3334.

[8] A. H. Castro Neto, F. Guinea, N. M. R. Peres, K. S. Novoselov, and A. K. Geim, *The electronic properties of graphene*. Rev. Mod. Phys. 81, 109.

[9] F. H. L. Koppens, D. E. Chang, and F. J. García de Abajo, *Graphene Plasmonics: A Platform for Strong LightMatter Interactions*. Nano Letters 2011 11 (8), 3370-3377.

[10] E. Hendry, P. J. Hale, J. Moger, A. K. Savchenko, and S. A. Mikhailov, *Coherent Nonlinear Optical Response of Graphene*. Phys. Rev. Lett. 105, 097401.

[11] S. A. Mikhailov, *Electromagnetic response of graphene: Non-linear effects*. Physica E 40, 2626-2629 (2008).

[12] M. Jablan, M. Soljacic and H. Buljan, *Plasmons in Graphene: Fundamental Properties and Potential Applications*. Proceedings of the IEEE , vol.101, no.7, pp.1689,1704, July 2013.

[13] A. Yu. Nikitin, T. Low, and L. Martin-Moreno, *Anomalous reflection phase of graphene plasmons and its influence on resonators*. Phys. Rev. B 90, 041407(R).

[14] J. Chen, M. Badioli, P. Alonso-González, S. Thongrattanasiri, F. Huth, J. Osmond, M. Spasenović, A. Centeno, A. Pesquera, P. Godignon, A. Zurutuza Elorza, N. Camara, F. J. García de Abajo, R. Hillenbrand and F. H. L. Koppens, *Optical nano-imaging of gate-tunable graphene plasmons*. Nature 487, 7781.

[15] Z. Fei, A. S. Rodin, G. O. Andreev, W. Bao, A. S. McLeod, M. Wagner, L. M. Zhang, Z. Zhao, M. Thiemens, G. Dominguez, M. M. Fogler, A. H. Castro Neto, C. N. Lau, F. Keilmann and D. N. Basov, *Gate-tuning of graphene plasmons revealed by infrared nano-imaging*. Nature 487, 8285.

[16] U. Fano, *Effects of Configuration Interaction on Intensities and Phase Shifts*. Phys. Rev. 124, pp. 18661878.